

# Telescoping Jet Substructure

Yang-Ting Chien<sup>a,d,\*</sup>, Alex Emerman<sup>c,d,e</sup>, Shih-Chieh Hsu<sup>b</sup>, Samuel Meehan<sup>b</sup>, and Zachary Montague<sup>a,b</sup>

<sup>a</sup> *Center for Theoretical Physics, Massachusetts Institute of Technology, Cambridge, MA 02139*

<sup>b</sup> *Department of Physics, University of Washington, Seattle, WA 98195*

<sup>c</sup> *Department of Physics, Columbia University, New York, NY 10027*

<sup>d</sup> *Theoretical Division, T-2, Los Alamos National Laboratory, Los Alamos, NM 87545*

<sup>e</sup> *Physics Department, Reed College, Portland, OR 97202*

(Dated: November 21, 2017)

We introduce a novel jet substructure calculus which exploits the variation of observables with respect to a sampling of phase-space boundaries quantified by the variability. We apply this method to identify boosted  $W$  boson and top quark jets using telescoping jet grooming and telescoping subjets, demonstrating its ability to disentangle information coming from subjet topology and that coming from subjet substructure. We find excellent performance of the variability, in particular its robustness against finite detector resolution. This method provides a new direction in heavy particle tagging and enables a complete and systematic approach to the decomposition of jet substructure.

The Large Hadron Collider (LHC) has begun to probe physics above the electroweak scale, where the momenta of massive Standard Model particles are much larger than their invariant masses, resulting in hadronic decays of jets with prong-like substructures. Many jet substructure variables have been designed [1–3] and combined using multivariate techniques [4–7] to identify such jets and increase the sensitivity to beyond the Standard Model physics. The ability to reconstruct the features of such jets accurately is obscured by the presence of additional proton-proton interactions, i.e. pileup, as well as the underlying event of the hard collision, both of which cause additional radiation to fall within the catchment area of the jet. Often, this radiation is removed through a grooming procedure, e.g. pruning [8] or trimming [9]. Jet substructure observables and grooming procedures target certain intuitive features of the radiation properties and often have tuneable parameters. For example, the pruning parameters  $z_{\text{cut}}$  and  $D_{\text{cut}}$  control the softness and noncollinearity of a discarded particle. Conventionally, one makes a single choice of parameters deemed optimal by some metric. However, such a choice may neglect the full information the entire observable class contains.

Recently, Q-jets [10] introduced non-determinism in jet clustering. The procedure probes each jet multiple times and quantifies differences among pruned jets using the mass volatility. Later, telescoping jets [11] probed the radiation pattern surrounding the dominant energy flow with multiple angular resolutions  $\{R_i\}$  and extracted the full information contained in jets at all angular scales. In this Letter, we apply telescoping jets to analyze a set of commonly used jet observables and grooming procedures. We demonstrate the feasibility of this method as applied to the identification of hadronically decaying  $W$  bosons and top quarks. The mass volatility in Q-jets is promoted to the variability of each observable induced by the variation of its parameters.

In hadronic boosted two-body resonance decays, such as that from a  $W$  boson, the resonance mass  $M$  intro-

duces a two-prong structure in the jet at an angular scale  $\Theta \approx 2M/p_T$  between the two prongs, where  $p_T$  is the transverse momentum of the heavy particle. On the other hand, QCD jets initiated by isolated quarks and gluons do not have such a distinct scale. However, when examining jets with masses near  $M \pm \Delta m$ , QCD jets are also two-prong-like but with a more distended radiation pattern when  $\Delta m \gg \Gamma$ , where  $\Gamma$  is the natural width of the resonance. Besides this nontrivial *subjet topology*, the strong interaction dictates the formation of subjets with *subjet substructures* and *subjet superstructures* [12] which are sensitive to the partonic origins of subjets.

In the case of boosted top quarks, the top mass ( $M_t$ ) and the  $W$  mass ( $M_W$ ) are not hierarchically separated. Therefore  $\Theta_t \approx 2M_t/p_T^t$  and  $\Theta_W \approx 2M_W/p_T^W$  can be comparable. This results in the generic three-prong structure in the hadronic top decay  $t \rightarrow W + b \rightarrow q_1 + q_2 + b$ . However, when examining jets with a mass near  $M_t \pm \Delta m$  the selected QCD jets are, again, two-prong-like, so observables which distinguish three-prong jets from two-prong jets will help discriminate QCD jets from true top quark jets.

Given an arbitrary jet observable  $\mathcal{O}$  with a parameter  $a$ , the variation of the observable with respect to the sampling of parameters  $\{a_i\}$  within  $(a_{\text{min}}, a_{\text{max}})$ , or the *variability*, is quantified by the coefficient of variation  $v_{\mathcal{O}}^a$  defined as the ratio of the standard deviation and the mean of  $\{\mathcal{O}_{a_i}\}$ ,

$$v_{\mathcal{O}}^a = \frac{\sigma(\mathcal{O}_{a_i})}{\langle \mathcal{O}_{a_i} \rangle}. \quad (1)$$

Variations with respect to multiple varied parameters can be studied using the variability matrix. Much like the first derivative in calculus, the variability  $v_{\mathcal{O}}^a$  measures the change of the observable  $\mathcal{O}$  with respect to the change of the phase-space boundary set by the parameter  $a$ . Instead of combining observables with different parameters in a multivariate analysis, the variability can give a trend of the observable variation which itself can be used as a

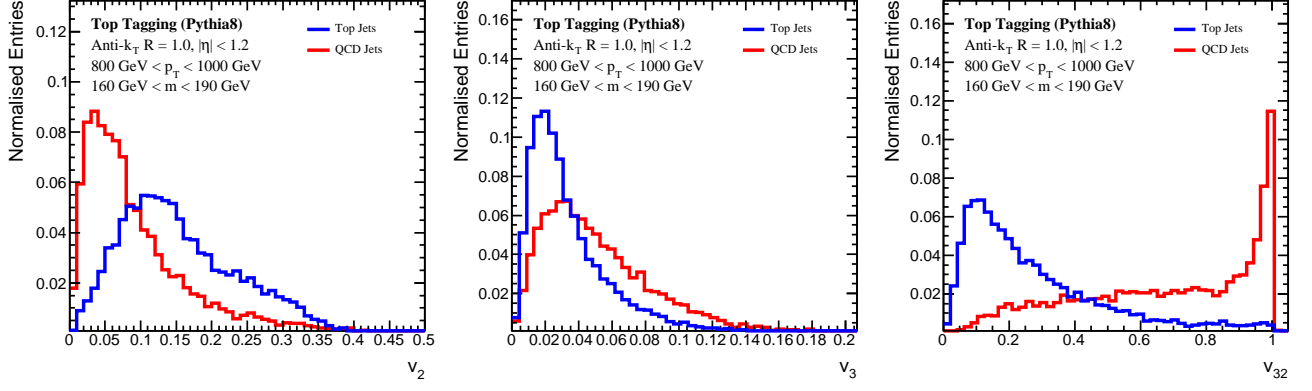


FIG. 1. The distributions of the variabilities  $v_2$  (left panel) and  $v_3$  (middle panel), as well as their ratio  $v_{32}$  (right panel) for top and QCD jets with  $800 \text{ GeV} < p_T < 1 \text{ TeV}$  and  $160 \text{ GeV} < m < 190 \text{ GeV}$  using the truth-particle information.

distinguishing feature to classify jets.

We consider a variety of telescoping applications. We focus on the variability of the jet mass with respect to varying the parameters which determine the constituents contributing to the jet mass. The sampling of the telescoping parameters is uniform within the range  $(a_{\min}, a_{\max})$ .

**Telescoping subjects:**  $N$  subjects are reconstructed exclusively around dominant energy flows within a jet. A similar method using the leading subjects in a reclustered jet was explored in [13]. We choose the subject axes as the  $N$ -subjettiness axes [14] with  $\beta = 1$  and build subjects around them with radius  $R_T$  [15–18]. Particles are assigned to the nearest axis according to the distance  $\Delta R_{ij}$  between the axis  $\hat{n}_i$  and particle  $p_j$ ,

$$\text{subject}_i = \{p_j \mid \Delta R_{ij} < R_T \text{ and } \Delta R_{ij} < \Delta R_{kj}, \forall k \neq i\}, \quad (2)$$

where  $k$  is the index of the other axes  $\hat{n}_k$ . The variability  $v_N$  of the invariant masses of the sum of  $N$  subjects is reconstructed with the telescoping parameter  $a = R_T \in (0.1, 1.0) \times R$ . Note that  $a_{\max}$  is chosen to be the jet radius  $R$  to scan through the entire catchment area of the jet. On the other extreme, the dominant energy features will be lost if  $a$  is too small, so  $a_{\min}$  is chosen as  $0.1 \times R$ . We focus on  $N = 2$  and  $3$  in  $W$  and  $N = 2, 3$ , and  $4$  in top tagging, but  $N$  could be extended further for more exotic boosted topologies.

**Telescoping pruning:** using the  $k_T$  reclustering algorithm, pruning discards soft and noncollinear particles when merging particles  $i$  and  $j$  if the combination is both soft and wide-angled,

$$\frac{\min(p_{T_i}, p_{T_j})}{|p_{T_i} + p_{T_j}|} < z_{\text{cut}} \quad (\text{soft})$$

$$\Delta R_{ij} > D_{\text{cut}}, \quad (\text{noncollinear}) \quad (3)$$

where  $p_{T_i}$  are the particle transverse momenta and  $\Delta R_{ij} = \sqrt{\Delta y_{ij}^2 + \Delta \phi_{ij}^2}$  is the distance between the

particles  $i$  and  $j$  with rapidity  $y$  and azimuthal angle  $\phi$ . We fix  $z_{\text{cut}} = 0.1$  and construct  $v_{\text{prun}}$ , the variability of the pruned jet mass with the telescoping parameter  $a \in (0.1, 2.0)$  in  $D_{\text{cut}} = a \cdot 2m_{\text{jet}}/p_{T_{\text{jet}}}$ .

**Telescoping trimming:** trimming reclusters jets into subjects using the  $k_T$  algorithm with subject radius  $R_{\text{sub}}$ . The subject  $i$  is discarded if it is soft, i.e.

$$p_{T_i} < f_{\text{cut}} p_{T_{\text{jet}}} \cdot (\text{soft}) \quad (4)$$

Here  $p_{T_i}$  is the transverse momentum of the  $i^{\text{th}}$  subject. We construct  $v_{\text{trim}}$ , the variability of the trimmed jet mass with the telescoping parameter  $a = f_{\text{cut}} \in (0.0, 0.1)$ .

Besides variabilities, useful angular observables, which encode information about subject topology, and mass observables, which reveal the presence of specific decay products, can be obtained seamlessly from the telescoping subject algorithm. For instance, in  $W$  tagging with  $N = 2$ , subject topology is affected by the jet mass cut, but  $W$  and QCD jets can still have significantly different distributions for the angle  $\theta_2$  between the two dominant energy flows. For top tagging with  $N = 3$ , we consider the minimal angle  $\theta_{\min}$  among the subject axes. For QCD jets, this angle is expected to be small while for top jets it will be distributed away from zero. Also, we attempt to identify the  $W$  inside the top jet [19, 20] by considering  $m_{W2}$ , the invariant mass of two of the three exclusive voronoi regions closest to the  $W$  mass, and its variability  $v_{m_{W2}}$  by scanning within those two regions.

The study is performed using samples generated from Monte Carlo simulations of proton-proton collisions at  $\sqrt{s} = 13 \text{ TeV}$  using PYTHIA8 [21]. Particles are clustered into jets with FASTJET 3 [22] using the anti- $k_T$  algorithm [23] with  $R = 1.0$  and are required to be central with a pseudorapidity  $|\eta| < 1.2$ . We consider two kinematic regimes where the jet  $p_T$  is either between 350 GeV and 500 GeV or 800 GeV and 1 TeV. Signal  $W$  boson and top quark jets are generated using decays of heavy Kaluza-Klein gravitons with invariant masses at 1 or 2

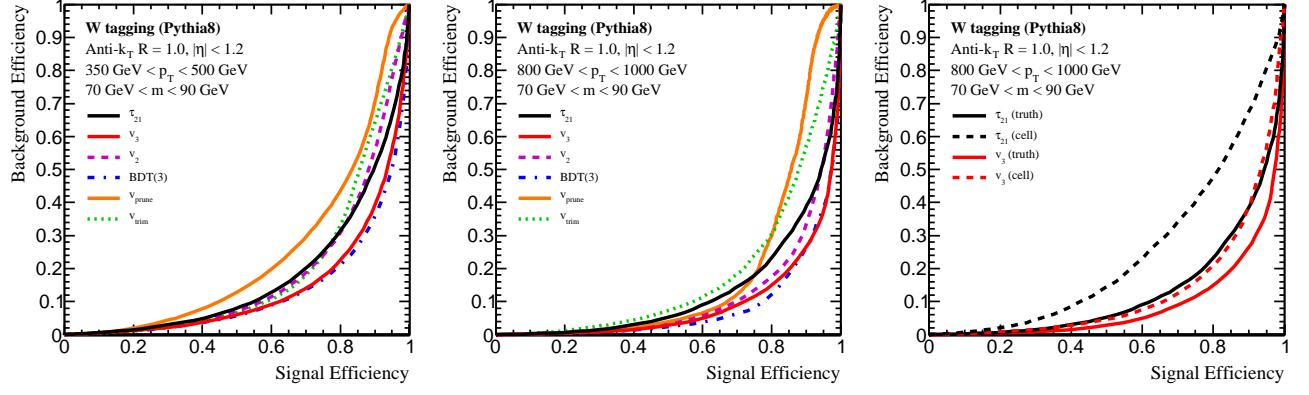


FIG. 2. The  $W$  tagging ROC curves of the variabilities  $v_2$ ,  $v_3$ ,  $v_{\text{trim}}$ , and  $v_{\text{prun}}$ ; the BDT combinations of three telescoping subjets variables  $\{v_2, v_3, \theta_2\}$ ; and the two-prong tagger  $\tau_{21} = \tau_2/\tau_1$  in the (300 GeV, 500 GeV) jet  $p_T$  bin (left panel) and the (800 GeV, 1 TeV) bin (middle panel). Right panel: ROC curves of  $v_3$  and  $\tau_{21}$  in the (800 GeV, 1 TeV) jet  $p_T$  bin. Solid curves correspond to the ones with the truth-particle information, and the dashed curves are the ones using the pseudo-calorimeter cell particle information.

TeV for the two  $p_T$  bins in  $gg \rightarrow G^* \rightarrow W^+W^-$  or  $t\bar{t} \rightarrow 191$  hadrons. Background QCD jets are generated from the 192 Standard Model dijet process. To study the impact of 193 finite detector resolution, we compare the results with 194 the particles clustered in pseudo-calorimeter  $(\eta, \phi)$  cells 195 of size  $0.1 \times 0.1$ , with each cell momentum constructed 196 with zero mass and direction from the primary vertex. 197 Although we do not include pileup in our studies, using 198 groomed jet constituents can mitigate the pileup effect. 199 In the case of telescoping subjets, jets are groomed using 200 the trimming algorithm with  $R_{\text{sub}} = 0.3$  and  $f_{\text{cut}} = 0.05$ . 201 A selection on the trimmed jet mass is made between 70 202 GeV and 90 GeV for  $W$  tagging and between 160 GeV 203 and 190 GeV for top tagging. 204

To examine the complementarity of the information 205 contained in the telescoping subjet variables, subsets 206 of them are inputs for Boosted Decision Trees (BDTs) 207 implemented in TMVA [24]. For top tagging we also 208 consider the ratio  $v_{N2}$  between  $v_N$  and  $v_2$  for  $N = 3, 4$ , 209

$$v_{N2} = \frac{v_N}{v_2}. \quad (5) \quad 210 \quad 211 \quad 212$$

Shown in Figure 1 are the distributions of  $v_2$ ,  $v_3$ , and 213  $v_{32}$  for top and QCD jets. We find that top jets have a 214 broader  $v_2$  distribution and a narrower  $v_3$  distribution. 215 The large variation of the jet mass when telescoping 216 around the two subjet axes is caused by the transition of 217 the  $W$  from being partially reconstructed to fully recon- 218 structed. There is not an intrinsic mass scale dictating 219 the third hard emission for QCD jets. On the other 220 hand, the three prongs inside top jets are quark-initiated 221 subjets, whereas the subjets in QCD jets can have gluonic 222 origins. Quark subjets are narrower than gluon subjets; 223 therefore  $v_3$  of top jets is statistically smaller.  $v_{32}$  has 224 almost the same performance as the BDT with input 225  $\{v_2, v_3\}$ , suggesting that  $v_{32}$  may be the optimal way of 226

combining the two variabilities.

An interesting feature of  $v_{32}$  is that it cuts off naturally at 1, most clearly seen in QCD jets. Crucially,  $v_3 \leq v_2$ . The two-prong structure in QCD jets implies that  $v_2$  and  $v_3$  collect similar information. The third energy flow axis can not be displaced far from the two axes determined at  $N = 2$ . Hence, little new information is collected by constructing a third subjet and the distribution of  $v_{32}$  for QCD jets peaks at 1. In the case where there is a third, semi-hard emission, the emission is captured by all telescoping subjets at  $N = 3$  and does not induce the observable variation and so  $v_3 < v_2$ . In general, for larger  $N$ , more particles are captured by-default and so the variability is expected to decrease ( $v_{N+1} \leq v_N$ ).

The performances of the observables are illustrated by receiver operating characteristic (ROC) curves, plotting the background efficiency as a function of the signal efficiency, where a lower curve indicates a better tagging performance. Shown in Figure 2 are the ROC curves of  $v_2$ ,  $v_3$ ,  $v_{\text{trim}}$ ,  $v_{\text{prun}}$ , the BDT combinations of the telescoping subjet variables  $\{v_2, v_3, \theta_2\}$ , and the two-prong tagger  $\tau_{21} = \tau_2/\tau_1$  in  $W$  tagging. The left and middle panels correspond respectively to two jet  $p_T$  regions of (350 GeV, 500 GeV) and (800 GeV, 1 TeV). Overall, the tagging performance increases at higher  $p_T$ , demonstrating the general advantage of applying telescoping deconstruction to the boosted regime. We find excellent performance of  $v_3$  and its qualitatively different feature compared to  $\tau_{21}$ . In the right panel, we compare the tagging performance using truth particles and pseudo-calorimeter clusters, which degrade information about structures smaller than the cell size. We find that  $v_3$  is much more robust against this smearing, especially at high  $p_T$ . The  $v_3$  observable utilizes the  $W$  isolation and probes the rapid depletion of radiation around the  $W$  at larger angles in the boosted regime. This is the

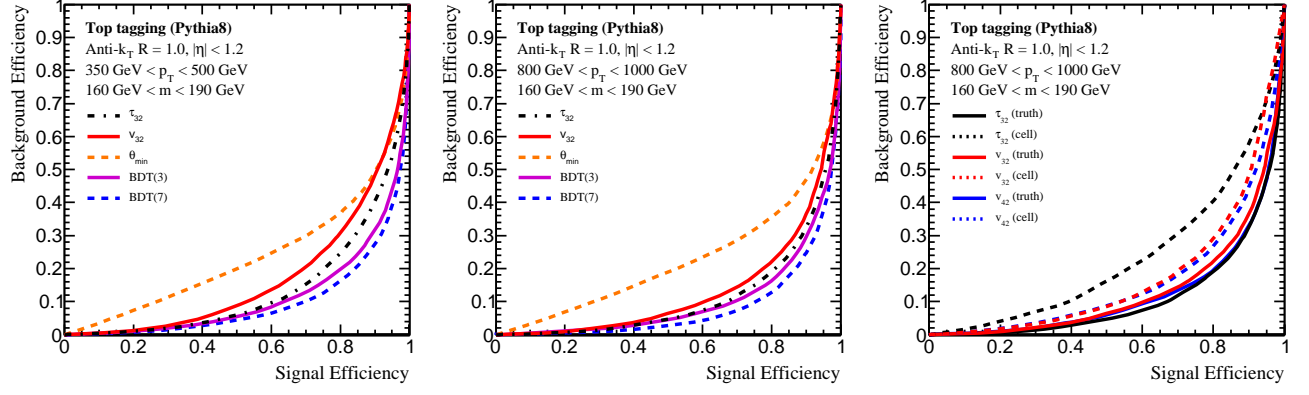


FIG. 3. The top tagging ROC curves of the variability ratio  $v_{32}$ , the minimal angle among three subjects  $\theta_{\min}$ , the BDT combinations of three and seven telescoping subjects variables  $\{m_{W2}, v_2, v_3\}$  and  $\{\theta_2, \theta_{\min}, m_{W2}, v_2, v_3, v_4, v_{m_{W2}}\}$ , and the three-prong tagger  $\tau_{32} = \tau_3/\tau_2$  in the (300 GeV, 500 GeV) jet  $p_T$  bin (left panel) and the (800 GeV, 1 TeV) bin (middle panel). Right panel: ROC curves of  $v_{32}$ ,  $v_{42}$  and  $\tau_{32}$  in the (800 GeV, 1 TeV) jet  $p_T$  bin. Solid curves correspond to the ones with the truth-particle information, and the dashed curves are the ones using the pseudo-calorimeter cell particle information.

manifestation of the fact that the  $W$  carries zero color charge which affects the color structure of the subjects. The time dilation that occurs before  $W$  hadronically decays can also create a huge difference from QCD jets in the jet formation process. On the other hand, the fact that  $v_3$  performs better than  $v_2$  hints at the significance of a third, semi-hard emission in  $W$  and QCD jets;  $v_3$  disentangles that effect in the quantification of the  $W$  isolation. Neither  $v_{\text{prun}}$  nor  $v_{\text{trim}}$  are as effective as  $v_2$  or  $v_3$  in the boosted regime. However, they demonstrate the generality of the telescoping algorithm and may have improved performance with further optimizations conducted on the choices of ranges for the grooming parameters.

Shown in Figure 3 are the ROC curves for top tagging performance including  $v_{N2}$  ( $N = 3, 4$ ),  $\theta_{\min}$ , the BDT combinations of telescoping subjects variables  $\{v_2, v_3, m_{W2}\}$  and  $\{\theta_2, \theta_{\min}, m_{W2}, v_2, v_3, v_4, v_{m_{W2}}\}$ , and the three-prong tagger  $\tau_{32} = \tau_3/\tau_2$ . Again, the left and middle panels correspond to the two kinematic regimes  $p_T \in (350 \text{ GeV}, 500 \text{ GeV})$  and  $p_T \in (800 \text{ GeV}, 1 \text{ TeV})$ , and we note tagging performance increases at higher  $p_T$ . In the right panel, the ROC curves plot both truth-particle and pseudo-calorimeter information. We find excellent performance of  $v_{N2}$  and its robustness against smearing, especially at high  $p_T$  where the performance of the more conventionally used  $\tau_{32}$  observable degrades dramatically. This indicates the qualitatively different features of  $v_{N2}$  and a three-prong tagger.  $v_{42}$  has a better performance than  $v_{32}$ , suggesting the significance of a fourth, semi-hard emission in top jets. One would also start to see the  $W$  isolation within the top jet in the boosted regime. We also find the usefulness of including  $m_{W2}$  in the minimal BDT combination which significantly increases the tagging performance. It is clear that the intrinsic mass scale  $M_W$  within the top

jet is a unique feature distinguishing itself from the QCD background.

To conclude, we introduce a qualitatively new jet substructure calculus using variability to quantify the change of observables with respect to a sampling of the phase-space boundaries in the observable definition. This method is general and can be used to analyze arbitrary classes of jet substructure observables and grooming procedures. In this context of  $W$  and top tagging, we find excellent performance, especially in the case of telescoping subjects, quantified by  $v_3$  in  $W$  tagging and  $v_{42}$  in top tagging. Furthermore, their robustness is found to be significantly better than more widely used  $N$ -prong taggers such as  $N$ -subjettiness via a comparison of the performance between reconstruction from using truth particles and from a pseudo-calorimeter.

The new physics messages we learn include the emergence of the isolation of  $W$  jets at high  $p_T$ , which is a dominant feature over their two-prong structure. This is true for all other heavy, color-singlet Standard Model particles including the  $Z$  and the Higgs boson. The top jet also has features beyond the three-prong structure which can be exploited to increase tagging performance. The telescoping subjects provides a systematic framework within which one can construct qualitatively new jet substructure observables. This paves the road toward complete and systematic jet studies using telescoping deconstruction [25].

## ACKNOWLEDGEMENTS

Y.-T. Chien would like to thank the organizers of the BOOST2015 conference where telescoping jet substructure was first presented. Y.-T. Chien was supported by the US Department of Energy (DOE), Office

of Science under Contract No. DE-AC52-06NA25396, the DOE Early Career Program and the LHC Theory Initiative Postdoctoral Fellowship under the National Science Foundation grant PHY-1419008. A. Emmerman was supported by the National Science Foundation under Grant No. PHY-1707971. S.-C. Hsu and S. Meehan were supported by the DOE Office of Science, Office of High Energy Physics Early Career Research program under Award Number DE-SC0015971. Z. Montague was supported by the University of Washington's Ernest M. Henley & Elaine D. Henley Endowed Fellowship.

---

\* ytchien@mit.edu

- [1] A. Abdesselam *et al.*, *Boost 2010 Oxford, United Kingdom, June 22-25, 2010*, Eur. Phys. J. **C71**, 1661 (2011), arXiv:1012.5412 [hep-ph].
- [2] A. Altheimer *et al.*, *BOOST 2011 Princeton, NJ, USA, 22-26 May 2011*, J. Phys. **G39**, 063001 (2012), arXiv:1201.0008 [hep-ph].
- [3] A. Altheimer *et al.*, *BOOST 2012 Valencia, Spain, July 23-27, 2012*, Eur. Phys. J. **C74**, 2792 (2014), arXiv:1311.2708 [hep-ex].
- [4] D. Adams *et al.*, Eur. Phys. J. **C75**, 409 (2015), arXiv:1504.00679 [hep-ph].
- [5] A. J. Larkoski, I. Moulton, and B. Nachman, (2017), arXiv:1709.04464 [hep-ph].
- [6] A. Collaboration (ATLAS Collaboration), (2017).
- [7] C. Collaboration (CMS Collaboration), JHEP **12**, 017, 43 p (2014), comments: Replaced with published version. Added journal reference and DOI.
- [8] S. D. Ellis, C. K. Vermilion, and J. R. Walsh, Phys.Rev. **D80**, 051501 (2009), arXiv:0903.5081 [hep-ph].
- [9] D. Krohn, J. Thaler, and L.-T. Wang, JHEP **1002**, 084 (2010), arXiv:0912.1342 [hep-ph].
- [10] S. D. Ellis, A. Hornig, T. S. Roy, D. Krohn, and M. D. Schwartz, Phys. Rev. Lett. **108**, 182003 (2012), arXiv:1201.1914 [hep-ph].
- [11] Y.-T. Chien, D. Farhi, D. Krohn, A. Marantan, D. Lopez Mateos, and M. Schwartz, JHEP **12**, 140 (2014), arXiv:1407.2892 [hep-ph].
- [12] J. Gallicchio and M. D. Schwartz, Phys. Rev. Lett. **105**, 022001 (2010), arXiv:1001.5027 [hep-ph].
- [13] Y. Cui, Z. Han, and M. D. Schwartz, Phys.Rev. **D83**, 074023 (2011), arXiv:1012.2077 [hep-ph].
- [14] J. Thaler and K. Van Tilburg, JHEP **03**, 015 (2011), arXiv:1011.2268 [hep-ph].
- [15] I. W. Stewart, F. J. Tackmann, and W. J. Waalewijn, Phys. Rev. Lett. **105**, 092002 (2010), arXiv:1004.2489 [hep-ph].
- [16] Y.-T. Chien, Phys. Rev. **D90**, 054008 (2014), arXiv:1304.5240 [hep-ph].
- [17] I. W. Stewart, F. J. Tackmann, J. Thaler, C. K. Vermilion, and T. F. Wilkason, JHEP **11**, 072 (2015), arXiv:1508.01516 [hep-ph].
- [18] J. Thaler and T. F. Wilkason, JHEP **12**, 051 (2015), arXiv:1508.01518 [hep-ph].
- [19] J. Thaler and L.-T. Wang, JHEP **07**, 092 (2008), arXiv:0806.0023 [hep-ph].
- [20] D. E. Kaplan, K. Rehermann, M. D. Schwartz, and B. Tweedie, Phys. Rev. Lett. **101**, 142001 (2008), arXiv:0806.0848 [hep-ph].
- [21] T. Sjostrand, S. Mrenna, and P. Z. Skands, Comput. Phys. Commun. **178**, 852 (2008), arXiv:0710.3820 [hep-ph].
- [22] M. Cacciari, G. P. Salam, and G. Soyez, Eur. Phys. J. **C72**, 1896 (2012), arXiv:1111.6097 [hep-ph].
- [23] M. Cacciari, G. P. Salam, and G. Soyez, JHEP **0804**, 063 (2008), arXiv:0802.1189 [hep-ph].
- [24] A. Hoecker, P. Speckmayer, J. Stelzer, J. Therhaag, E. von Toerne, and H. Voss, PoS **ACAT**, 040 (2007), arXiv:physics/0703039.
- [25] Y.-T. Chien, P. T. Komiske, and E. M. Metodiev, to appear soon (2017).